2016 24th International Lightning Detection Conference &
6th International Lightning Meteorology Conference
18 - 21 April | San Diego, California, USA

On the spatial structure of electric fields generated by clouds with simple charge structures

Christopher J. Biagi
Quasar Federal Systems
San Diego, CA
cbiagi@quasarfs.com

Kenneth L. Cummins
Department of Atmospheric Sciences
University of Arizona
Tucson, Arizona

***Abstract*— In this work we use quasi-static, finite-element modeling to examine the electric field structure outside of arbitrarily shaped clouds having a variety of internal charge distributions. We begin by examining the effect of screening layers on the electric fields outside of electrified clouds by comparing modeling results for charged clouds having electrical conductivities that are both equal to and lower than the surrounding clear air. As expected, the presence of a screening layer reduces the electric field magnitude outside of cloud boundaries, but the model comparisons indicate that the spatial structure of the electric field is approximately the same regardless of the difference in the conductivities between the cloud and clear air and the formation of a screening layer, even for altitude-dependent electrical conductivities. The similarity of the spatial structure of the electric field outside of clouds with and without a screening layer, with varying charge shapes, and with varying cloud boundary morphologies suggests that "bulk" properties related to cloud electrification, such as: (1) the center heights, (2) the separation distance, and (3) the charge magnitudes of charge centers, might be determined using measurements of the vector electric field at multiple locations in space outside the cloud and above ground.**

Keywords—screening layer, cloud charge, electric field

I. INTRODUCTION

It is becoming increasingly practical to employ small unmanned aerial vehicles (UAVs) to explore atmospheric electric fields in general, and more specifically electric fields in the vicinity of active thunderstorms. These low-cost platforms can fill an important gap in the observation of these electric fields [Nicoll, 2012]. Strides were made in our early understanding of electric fields both inside and outside of clouds using re-purposed military aircraft starting in the late 1940's (e.g., Gunn [1948]; Gunn [1957]), but these platforms were very expensive to operate. During the last 40 years, free-flight balloons have been used extensively to study electric fields and charge structure within thunderstorms (e.g., Marshall and Rust [1993]; Stolzenburg and Marshall [2008]), sometimes in combination with rockets (e.g., Marshall et al. [1995]). Balloons and rockets are less costly than manned aircraft, but are limited by their uncontrolled and mostly-vertical paths. Military and lower-cost commercial aircraft and sailplanes have been used in recent years (Breed and Dye [1989], Mo et al. [2003]; Dye et al. [2007]), but still at great cost. Large UAV's have been used to study the contribution of thunderstorm currents to the global circuit [Mach et al., 2009], but they have not been used for the study of developing and dissipating thunderstorms.

Small UAV's have important strengths and weaknesses when it comes to thunderstorm monitoring and/or research. They have the unique advantage that they are capable of very compact maneuvers, and they fly at appropriate speeds for observing thunderstorm dynamics. Historically, they have had limitations related to flight time and climb rate, but recent work as shown that these limitations can be mitigated (e.g., Zhang et al., this conference). One of the biggest concerns for SUAV's is their ability to maintain flight control and data quality while flying through turbulent and/or mixed-phase regions of a thunderstorm, given the small-scale instruments, low mass, and low forces associated with their control surfaces. These specific concerns have led us to take a fresh look at what can be learned about the structure of electrified clouds from the measurement of fields outside the cloud boundary. More specifically, we use modern finite-element modeling techniques to determine if measurements of the electric field along prescribed paths flight can be used to infer information about the existence and structure of charge within a cloud that may not be readily determined from measurements at the ground.

There is a long history of modeling currents and electric fields associated with electrical charge in thunderstorms. The basic physical properties of electrified clouds and characteristics of the measurement environment needed for this work have been broadly understood for nearly a century and summarized in a paper by C.T.R Wilson in 1956. A one-

dimensional mathematical model describing conduction currents produced by a thunderstorm was published by Holzer and Saxon in 1952. Over the ensuing decades, several models were developed with various objectives in mind (see Hayes and Roble [1979]; Tzur and Roble [1985]; Driscoll et al. [1992], and the references therein).

A broadly-accepted view is that one must penetrate a cloud in order to accurately determine the nature and distribution of charge within it. This is because clouds have a lower electrical conductivity than air and they develop layers of charge at their boundaries (screening layers) that mask the electric field produced by internal charge. Additionally, this screening is not uniform around the cloud, and depends on a variety of contributing factors [Marshall and Rust, 1991]. In this work, we use finite-element modeling to examine the effect of such screening layers, produced using a simple ohmic model of cloud electrical behavior, on electric fields outside of clouds of various geometries in order to better understand the utility of electric field measurements made near clouds with airborne platforms without cloud penetration.

The work presented here is an early step along a path toward detailed and realistic modeling of electrified clouds and the external fields that they produce, and does not include constraints on conduction current that are known to deviate from ohmic behavior [Krehbiel, 1969; Rust and Moore, 1974; Krehbiel, personal communication]. This work may eventually lead us to agree with historical perspectives about the need to penetrate a cloud in order to obtain accurate information about its charge distribution. Even if this is the case, our hope is to at least quantify the limits of near-cloud electric field observations for determining if a developing, stable or decaying cloud presents a risk for triggering lightning from aircraft penetrations or during space launch operations.

II. Model Description

The analyses described in this paper come from a two-dimensional, finite element model with axially symmetric geometry that is illustrated in Fig. 1. Unlike models employed in earlier studies, finite element modeling can represent any cloud shape because model elements can have arbitrary size and geometry. Fig. 1 shows the two general cloud shapes used in this study: a) a cumulonimbus (CB) shape, and b) a shape with thin depth but wide horizontal extent that approximates stratiform clouds (ST). The shape representing a CB cloud spans a vertical distance of 10 km with the cloud base at 3 km and the cloud top at 13 km. The horizontal span in the axisymmetric space varies from 3 km to 6 km, which corresponds to 6 km to 12 km in three-dimensional space. The side of the CB cloud has five bulges that are 2 km in height and have adjustable horizontal extent. The shape of the charge centers, which is also adjustable for different model studies, are a half circle or rectangle with a circular edge in axisymmetric space: these shapes correspond to a sphere or disk with a rounded edge in three dimensional space. The shape representing a ST cloud is similar to the CB cloud, but it has a depth of only 4 km. The positive and negative charge centers in the ST cloud shape are center at altitudes of 6 km and 4 km, respectively, and both have a depth of 1.9 km and a width of 4 km. Finally, for both cloud shapes, the overall

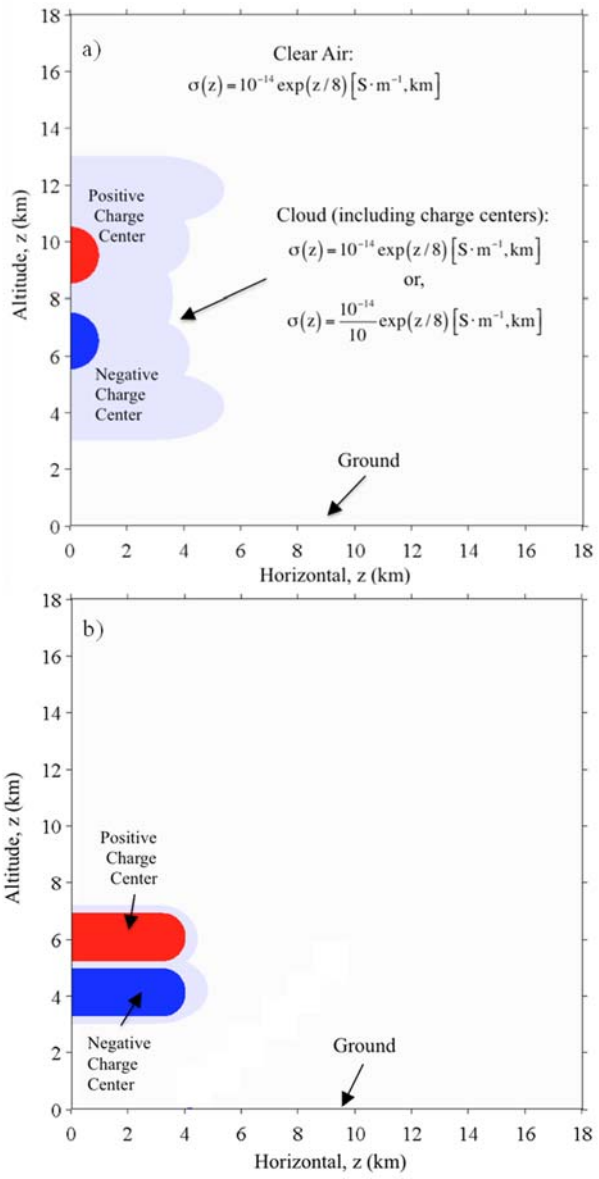

Fig.1 Model Geometry and Conductivity

model space has a horizontal (radial) and vertical extent of 18 km.

The model determines quasi-steady state solutions, assuming dB/dt is zero, to Gauss' law and the continuity equation given by Equations 1 and 2. The 'source current' term on the right side of Equation 2 represents the currents that are used to apply charge to the charge centers. Equation 3 indicates that the currents in the model are ohmic.

$$\vec{\nabla}\cdot\vec{E} = \frac{\rho}{\varepsilon_0} \qquad (1)$$

$$\frac{\partial \rho}{\partial t} + \vec{\nabla} \cdot \vec{J}_e = \text{Source Current} \quad (2)$$

$$\vec{J} = \sigma \vec{E}_e \quad (3)$$

The bottom horizontal axis is set to ground potential (V = 0 V), and the electric field values at the upper and right boundaries are relaxed to infinity using an infinite element boundary condition, and therefore to zero potential. The model reaches a quasi-steady-state and returns a solution when the source currents are balanced by the ohmic currents flowing between the charge centers, and from the charge centers to the outer boundaries of the model. The time-evolution of charges and electric fields are examined only for the ST cloud model.

The electrical conductivity throughout the model domain increases exponentially with height with a scale height of 8 km and a ground level value of 10^{-14} S m^{-1}: this is representative of reported measurements of vertical profiles of conductivity [Driscoll et al., 1992]. Anomalies within the lower boundary layer and differences in positive and negative conductivities are not included in the model. The model space is divided into clear air and cloudy air regions having independently adjustable electrical conductivities and height dependence. The cloudy air region includes the cloud and the two charge centers. The value of conductivity in the cloudy area is altered between that of clear air at an equivalent altitude, and the clear air value reduced by a factor of ten (equations describing the conductivity in both model regions are shown in Fig. 1a). Reducing the cloud conductivity requires reducing the charging current by a similar factor in order to achieve an equivalent charge in the charge centers. Henceforth, the case of cloudy air conductivity being lower than clear air by a factor of ten will be referred to as the "lower cloud conductivity" case, and the "equal cloud conductivity" case will refer to the cloud and air having equal conductivities. A more detailed discussion of the assumptions used in this model, and their shortcomings, is given in Section 5.

III. Model Results

Model results are presented in two-dimensional and one-dimensional plots. All of the two-dimensional plots have the same format and present the volumetric space charge density and electric field structure. The magnitudes of the space charge densities are presented by color surface plots using logarithmic scales that are normalized to the maximum space charge density values, which are given to the right of the color scales. The charge centers, which have significantly larger values of space charge density than the rest of the model space, have been omitted from these plots so that space charge density features in the cloud and clear air are more evident. The charge magnitudes were small (+/-10 C) to be consistent with clouds that do not produce breakdown fields. This resulted in quite small external electric fields. The radial and vertical components of the electric field are illustrated with black streamlines that show the overall structure of the electric field, but note that the spacing between streamlines does not correspond exactly to the field strength.

The one-dimensional plots display the electric field probed along linear paths that might represent, for example, flight paths followed by an instrumented UAV. Fig. 2 illustrates three paths - one diagonal, one vertical, and one horizontal - along which the modeled electric field is probed. Results for the diagonal path, which is oriented 45 degrees off the vertical and horizontal axes, are plotted against the product of the path length and the tangent of 45 degrees, which is equivalent to

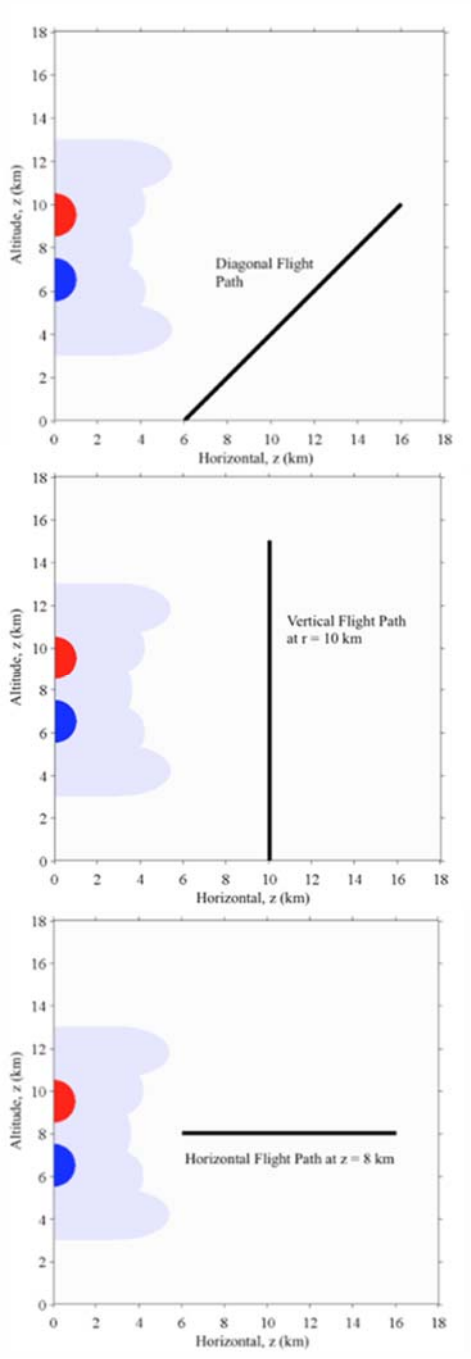

Fig. 2. Spatial Paths for probing electric field.

the r or z position relative to the start of the path at ground (where z = 0 km and r = 6 km). The one-dimensional line plots exhibit many features, including minimum and

maximum (extrema) points that are identified in the line plot graphs by shading and a point label. A total of 19 points are labeled in the line graphs, and analyses of these points are given in Section 4. Spatial locations where field values reverse polarity are also provided by the model, but these have not yet been analyzed.

Finally, in the one-dimensional plots, the magnitudes of the field values for the cases of equal cloud conductivity have been reduced by a factor of ten in order to plot them on the same vertical scale as the field values determined for the cases of lower cloud conductivity. This means that the screening layer reduces the magnitude of the electric field outside the cloud roughly (but not exactly) by a factor of ten, which is, appropriately, the same factor by which the cloud conductivity is reduced [Holzer and Saxon 1952].

A. Influence of Cloud Shape

The charge magnitude on the screening layer is not uniform since the current density and the cloud boundary shape both vary. Therefore, the electric field generated by the screening layer, which contributes to and distorts the electric field outside the cloud, depends on the current density and shape of the cloud boundary. The influence of cloud boundary shape on the formation of the screening layer and the electric field distortion outside the cloud was examined by varying the horizontal extent of the five bulges on the side boundary. A total of five different side boundaries were modeled for both cases of cloud conductivity. For all cases of side boundary and cloud conductivity, the generator current is set so that the steady-state solution is achieved when the upper and lower charge centers contain +10 C and -10 C of charge, respectively.

Two-dimensional model results for each of the five cloud boundary shapes (named Boundary 1 through 5) are shown in Fig. 3. The electric field and space charge distributions do not vary with changing cloud shape for the equal conductivity case, so results for the equal conductivity case are shown only for boundary 1 (inset a). Inset b shows the results for boundary 1 for the lower conductivity condition, and insets c through f show the results for the remaining cloud shapes employing the lower conductivity condition. Fig. 4 shows a vertical profile of the space charge density at a radius of 7 km from ground to an altitude of 18 km for the cloud geometry shown in Fig. 3e.

Some interesting inferences can be made from the model results shown in Fig. 3 and Fig. 4. A distribution of space charge develops in the cloudy and clear air that depends on the altitude-varying conductivity and is generally consistent with the electric field structure. Lines of minimum space charge density (colored dark blue) originate from each charge center and follow the two loci of the z-component reversals of the electric field. Fig. 4 shows that the polarity of space charge reverses across these minima lines. The space charge minima lines are distorted to varying extents near the cloud boundary for each cloud shape. The upper minimum originating from the positive charge center generally extends upwards and with increasing width. The lower minimum originating from the negative charge center curves toward and terminates at the ground at the so-called reversal distance [*Rakov and Uman*, 2003]. Henceforth, these features will be referred to the upper and lower reversal distances.

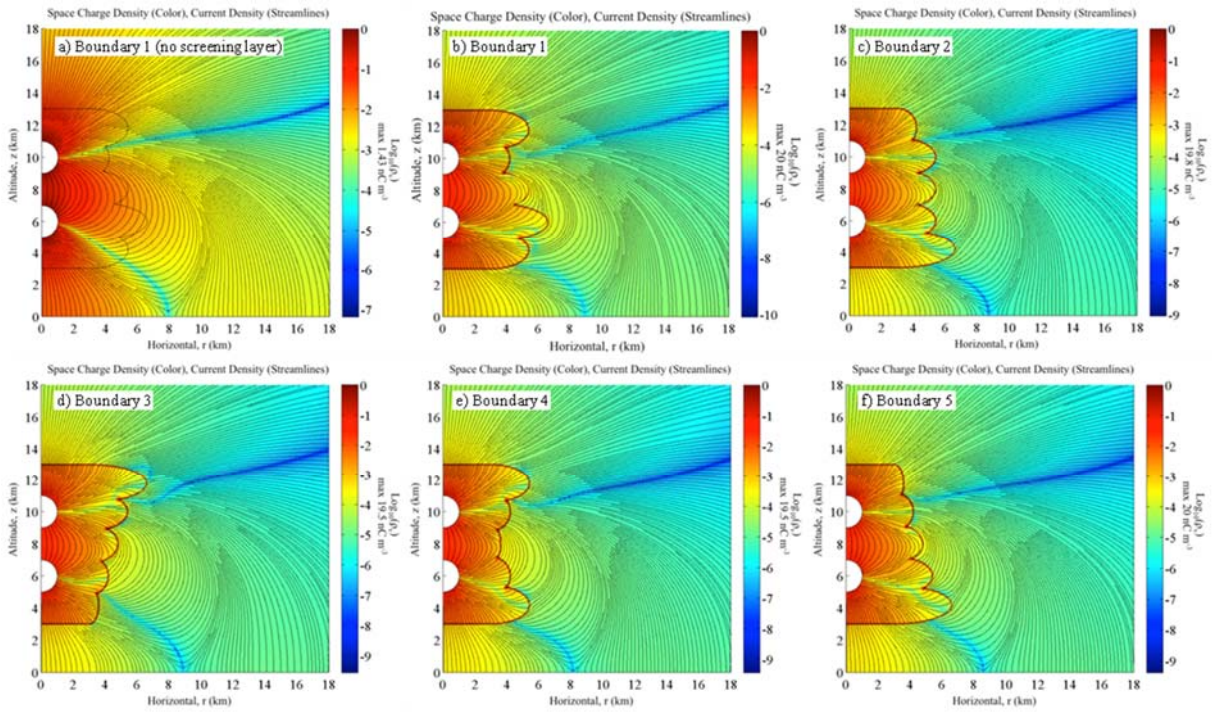

Fig. 3. Space charge density and electric field structure for varying side boundaries.

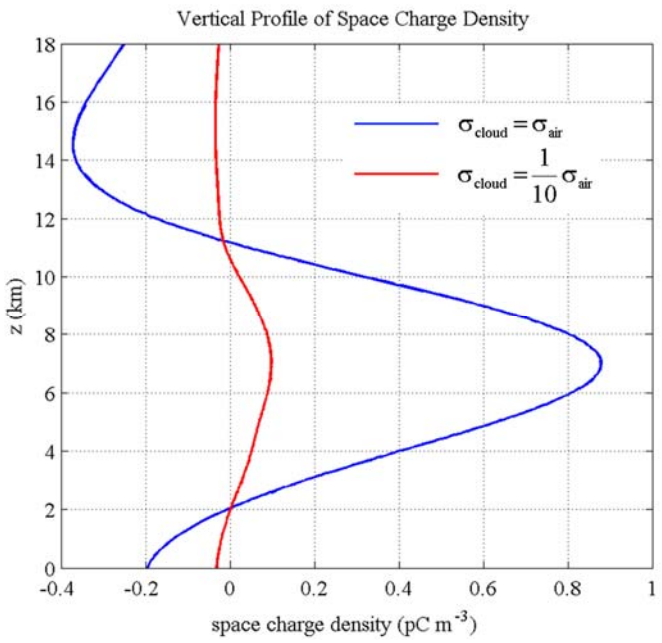

Fig. 4. Vertical profile of space charge density.

The reversal distance at ground for the equal conductivity case shown in Fig. 3a is approximately 8 km: this value is roughly 3 km less than value of 11 km predicted by Equation 3.4 in *Rakov and Uman* [2003]. If the altitude dependence of the conductivity were removed from the model (as assumed by *Rakov and Uman*), then the reversal distance would increase to 11 km. Therefore, the lower value of reversal distance at ground in the model results is due to the increase in conductivity with height and the resultant space charge distribution. Varying the side boundaries of the clouds in the lower conductivity cases changes the reversal distances at ground from about 8 km to 9 km. Additionally, at the cloud boundary, the location of the lower reversal distance varies in height from about 3 km to 5 km, and the location of the upper reversal distance remains relatively constant at 11 km. Both reversal distances are distorted significantly by the screening layer at locations very close to the cloud boundary. Additionally, at the cloud boundary, the location of the lower reversal distance varies in height from about 3 km to 5 km, and the location of the upper reversal distance remains relatively constant at 11 km. Both reversal distances are distorted significantly by the screening layer at locations very close to the cloud boundary.

It is clear in Fig. 3 that the screening layer on the cloud boundary has a significant impact on the space charge distribution and electric field profile near the cloud boundary. However, the influence of the screening layer decreases with increasing distance from the cloud boundary. The screening layer influence can be examined better in the one-dimensional graphs presented in Fig. 5 that show the total electric field, the radial field, and vertical field along the diagonal and horizontal flight paths (note the lines for the equal conductivity case are reduced by a factor of 10). The electric field profiles show remarkable similarity along both flight paths for all five cloud shapes, and for both cases of cloud conductivity. These results indicate that the effect of screening layers on the electric field structure outside of clouds (beyond a few km), including difference produced by widely varying cloud shape, is much less significant than the effect on the field magnitude.

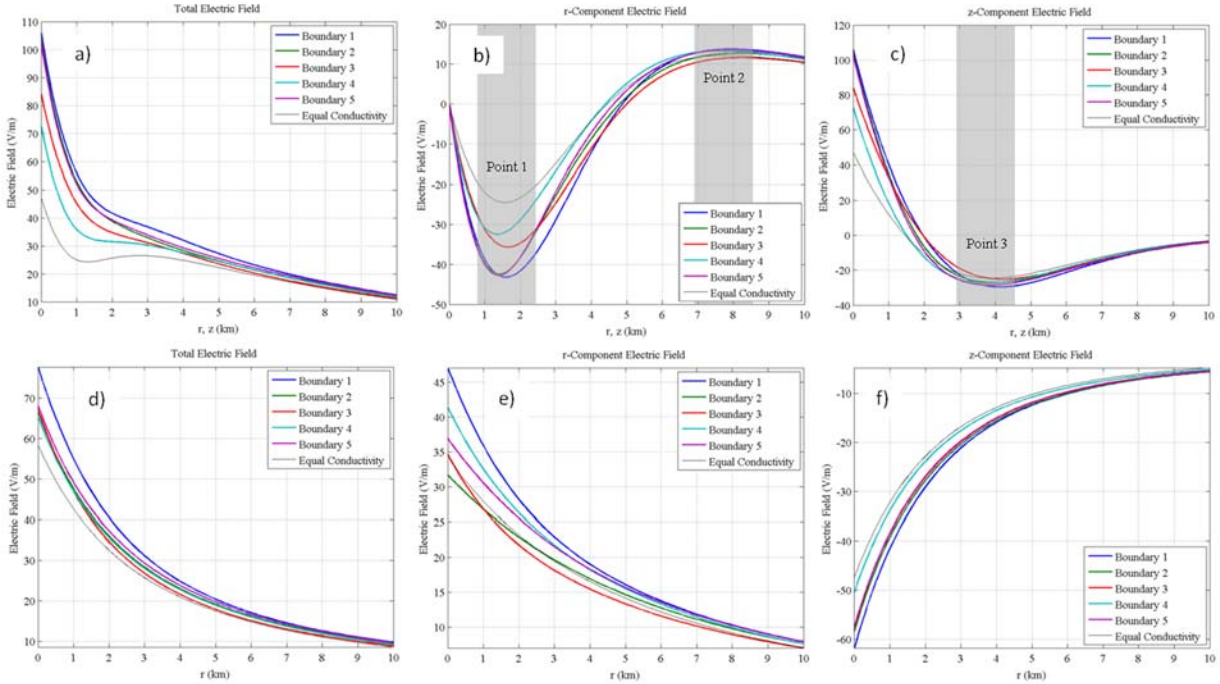

Fig. 5. The electric field along the diagonal path (top row) and vertical path (bottom row) for varying cloud boundaries.

If the electric field structure is similar with and without a screening layer, which these results indicate, then it is conceivable that that useful information regarding internal charge structures in clouds could be inferred using spatially resolved measurements of the electric field at altitude and, more importantly, outside clouds. For example, consider the electric field along the diagonal flight path that crosses the lower reversal distance in all the model cases (range of 1.5-2 km). The rate of change of the total electric field on the diagonal path (Fig. 5a) decreases significantly at altitudes above the lower reversal distance. Moreover, the r and z components exhibit extrema that could be measured easily. The r-component (Fig. 5b) reaches a maximum absolute value about where the z-component (Fig. 5c) crosses zero between about 1.5 km and 2 km. These features represent distinct data points that may be combined to reveal information about a cloud's internal charge structure: we analyze this possibility in Section 4.

B. Influence of Charge Separation

The influence of charge separation was examined by varying the height of the upper positive charge center in the cloud while maintaining the lower negative charge center at a fixed position centered at a height of 6 km. The four heights of the upper positive charge center were: 8 km, 9 km, 10 km, and 11 km. In each of the four cases, the charge magnitudes in the upper and lower charge centers were +10 C and -10 C, respectively. For this study, only the case of lower cloud conductivity was modeled, and the cloud had side boundary 4 (see Fig. 3e).

Two-dimensional model results for varying charge center separation are presented in Fig. 6. As the upper positive center height and the charge separation increase, the horizontal position of the reversal distance at ground increases (moves away from the cloud) and the height of the upper reversal distance increases. Although it is difficult to discern in Fig. 6, the screening layer charge at the upper and bottom boundaries increases with charge separation because the current density crossing these boundaries increases.

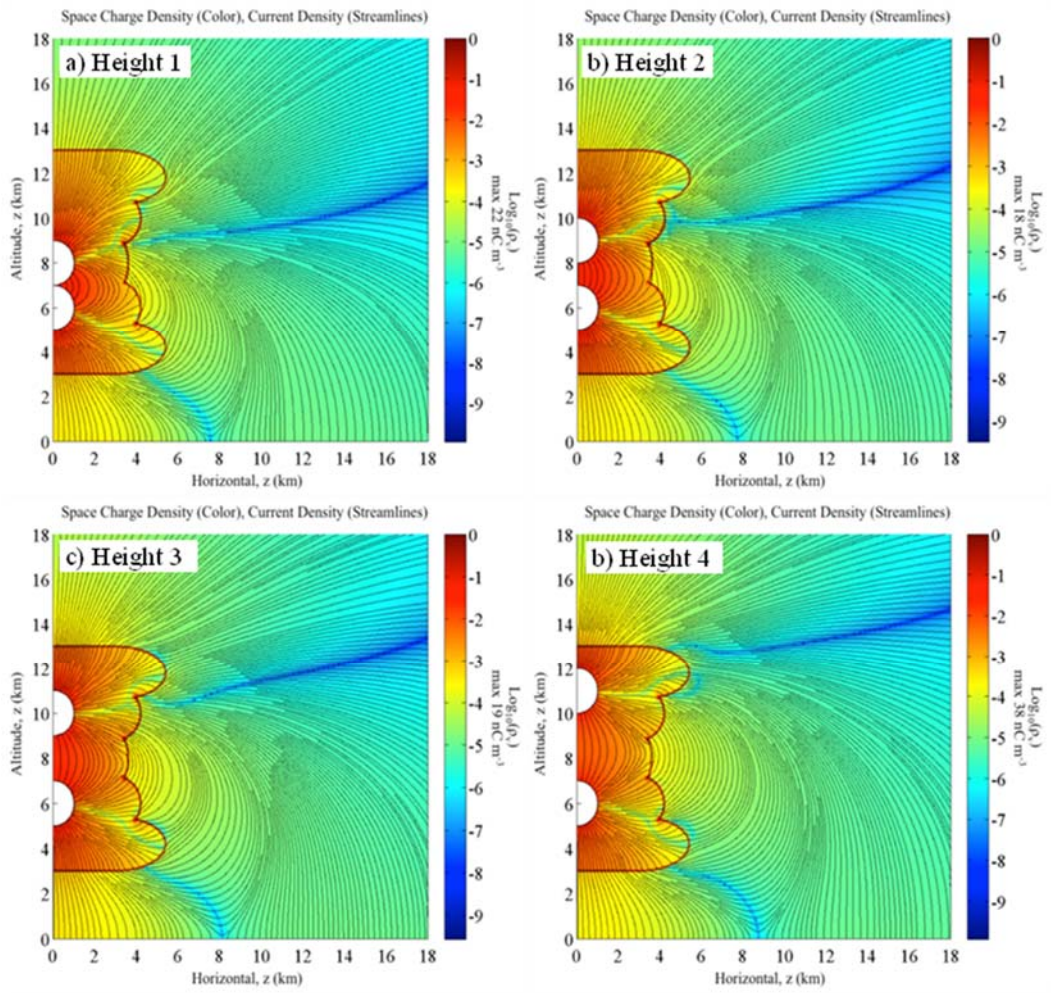

Fig 6. Space charge density and electric field structure for varying charge center separations.

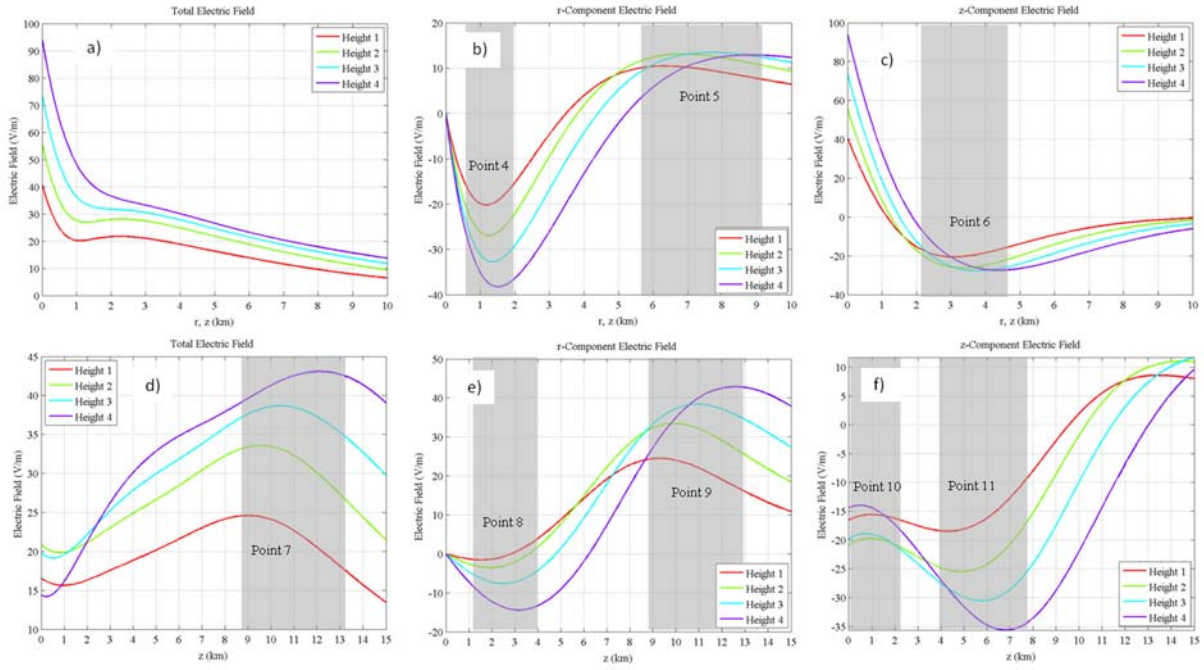

Fig. 7. The electric field along the diagonal path (top row) and horizontal path (bottom row) for different charge center separations.

Fig. 7 shows the electric field probed along the diagonal and vertical flight paths for the four cases of charge separation. Both electric field components evolve similarly along both flight paths, although there are clear differences in magnitudes and extrema locations.

As the charge separation increases: 1) the magnitude of the radial and vertical field components both increase, although the vertical component increases more than the radial component; 2) the reversal distances of both field components increase in r and z; 3) the locations of the extrema values in the radial and vertical field components increase in r and z; and 4) the magnitudes of the extrema values increase. These model results provide evidence that variations in charge separation distances can be monitored from outside of a cloud. Finally, the values of total electric field along the diagonal path (Fig. 7a) exhibit similar behavior for each charge separation distance, particularly for altitudes and radii below 500 m and above 3 km, where the rate of change of the fields in space (spatial gradient) are similar. As noted earlier, the behavior of the extrema indicated in the grey regions will be discussed in Section 4.

C. Influence of horizontal extent of charge

The influence of the horizontal extent, or the width, of the charge centers, was examined by modeling charge centers having widths of 1 km, 2 km, 3km, and 4 km in a cloud with Boundary 4 (see Fig. 3e). The charging current was adjusted for each charge center width so that the total charge magnitude in each center remained +/- 10 C. Two-dimensional model results for the four charge widths are given in Fig. 8. The left and right columns of Fig. 8 show the model results for the cases of equal and lower cloud conductivity, respectively, and charge center widths increases in successive rows.

The results given in Fig. 8 indicate that varying the charge center width has a relatively minor effect the electric field structure at distances greater than 1 km or so away from the cloud, and at ground. For example, the locations of the reversal distances at ground increase from about 8 km to 9 km over these extreme variations in charge width, and they are approximately the same for each case of cloud conductivity. The lower reversal distance changes more significantly at the cloud boundary for increasing charge widths, and also differently for the two cases of cloud conductivity. The upper reversal distance changes less significantly for increasing charge widths for both cases of cloud conductivity, although it does appear to be slightly lower in altitude for the case of lower cloud conductivity.

Fig. 9 shows the electric field probed along the diagonal (top row) and vertical flight (bottom row) paths for the four values of charge center widths and the two cases of cloud conductivity (note that the values for the equal conductivity case have been reduced by a factor of 10). The total, r-component, z-component, and zero-crossings of the electric fields evolve similarly on the flight paths for each charge width and each case of cloud conductivity. The magnitudes and locations of extrema values vary only slightly, even when a screening layer is present, other than the factor-of-10 reduction of the equal conductivity cases. Interestingly, the locations of the minimum and maximum values for both cases of cloud conductivity change by approximately the same amount as the charge width increases: this is best seen by examining the peaks in the total electric field values along the

vertical flight path between altitudes (z values) of 10 km and 12 km (labeled ‘Point 15’ in Fig. 9d).

For the cases with equal cloud conductivity, similar behavior is seen in the total electric field along the diagonal path (solid lines in Fig. 9a.) for each charge center width, although the absolute levels vary slightly. For the case of lower cloud conductivity (dashed lines in Fig. 9a.), the

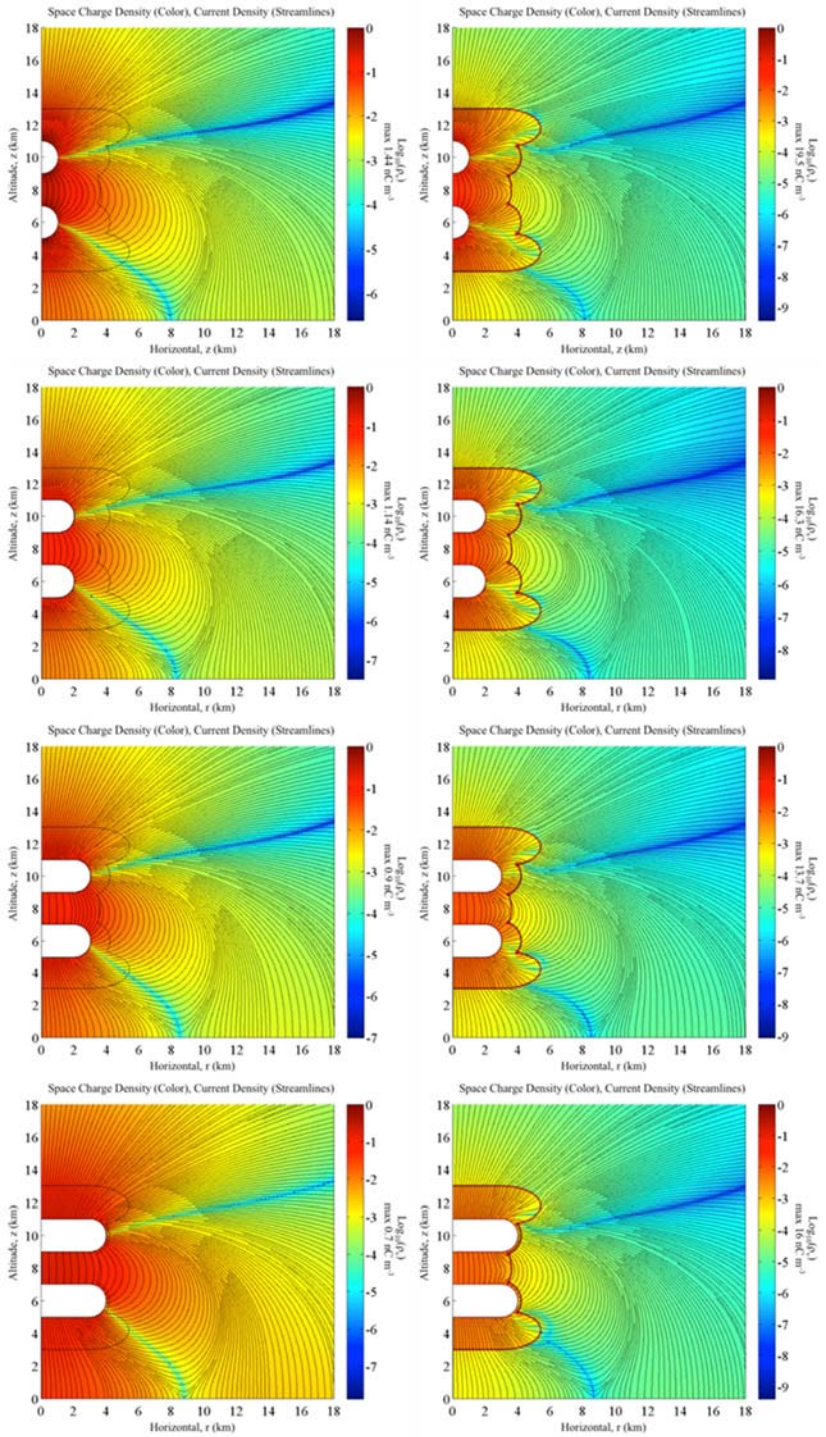

Fig. 8. The space charge density and electric field structure for varying charge center widths.

evolution of the total electric along the diagonal flight path is remarkably similar, particularly in the r and z range between 1 km and 2 km. For both cloud conductivity conditions, the spatial derivatives of the total electric fields along the diagonal path are similar for each charge width. These model results suggest that electric field measurements well-outside of a cloud will not be sensitive to the horizontal extent of the charge regions, for a fixed total charge.

D. Time evolution for strataform cloud

The results presented in the previous sections for cumulonimbus clouds were taken from quasi-steady state model solutions. In this section we present the modeled time-evolution for a cloud shape representing a mid-level strataform layer cloud with the geometry described in Section 2 and Fig. 1b. The upper positive and lower negative charge centers are symmetric, and they are charged with a current to attain steady state charges of +10 C and -10 C, respectively.

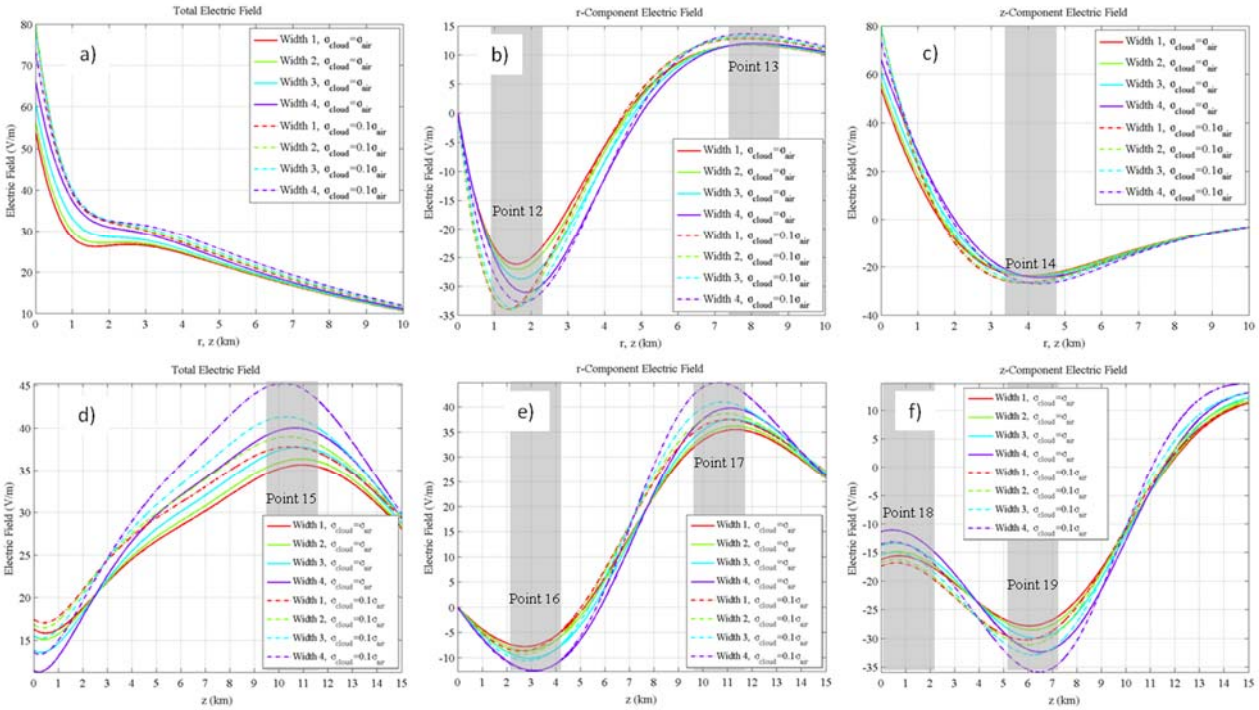

Fig. 9. The electric field along the diagonal path (top row) and horizontal path (bottom row) for varying charge widths

.

Fig. 10 shows the two-dimensional model results for the equal and lower cloud conductivity cases after the model has achieved steady state; the results are quite similar to those for the CB cloud shape. Two lines of minimum space charge density originate from the two charge centers. The upper line extends outwards and upwards, and the lower line curves toward and terminates at ground. The field reversal distance at ground increases by about 500 m when the cloud conductivity is reduced and a screening layer forms. The screening layer distorts the electric field near the cloud boundary, but much less distortion can be seen at distances of 1 km or greater from the cloud boundary.

Fig. 11 shows the time evolution of the spatially integrated space charge density in the charge centers for each case of cloud conductivity. Solid lines correspond to the equal conductivity case, and dashed lines correspond to the lower conductivity case. In the model, the charging currents are turned on at t = 0 min and turned off at about t = 165 min (10,000 s). For both conductivity cases, when the currents are turned on, the charge magnitudes increase exponentially, although the rate of charge increase is faster for the equal conductivity case, which has a higher charging current. When the charging currents are turned off, the charges decay exponentially, and again, more quickly for the equal conductivity case. The time evolution of the charge is consistent with the step response of an RC circuit, where the value of R is inversely proportional to the spatially dependent conductivity, and the value of C is governed by the geometry of the charge centers and the free-space permittivity. Clearly, the value of R is greater for the lower cloud conductivity case than for the equal conductivity case. Moreover, careful inspection of Fig. 11 shows that the rise time is faster for the upper positive charge center, which is consistent with its conductivity being greater than that of the lower negative charge center, which is at a lower altitude.

The relationship between the time-evolution and conductivity is also exhibited by the electric field outside the cloud. Fig. 12 shows the total electric field evolution in time at the six points along the diagonal path shown in Fig. 13. Fig. 12a shows the time evolution over 330 minutes, and Fig. 12b. shows an expanded view over the first 90 minutes. All of the electric field profiles are normalized to unity in order to emphasize the differences in time evolution. It is evident in Fig. 12 that the rate of change of electric field is different at each point; the rate is slowest near ground, and it increases with altitude and radius to point 6. These results are consistent with the conductivity increasing with altitude, or, alternatively, the resistance of the RC equivalent, and the associated time constant, decreasing with altitude. Fig. 14 shows the rise of electric field at point 6 for both cases of

cloud conductivity, and the time constants (the times at which the levels reach 63% of the peak) are identified. The time constant is about 68% greater for the lower conductivity case.

Finally, it is interesting to compare the times at which the charge centers and the electric fields at the six points attain a maximum, steady state value. For the equal conductivity case, the charge centers reach a steady state at a time of about 45

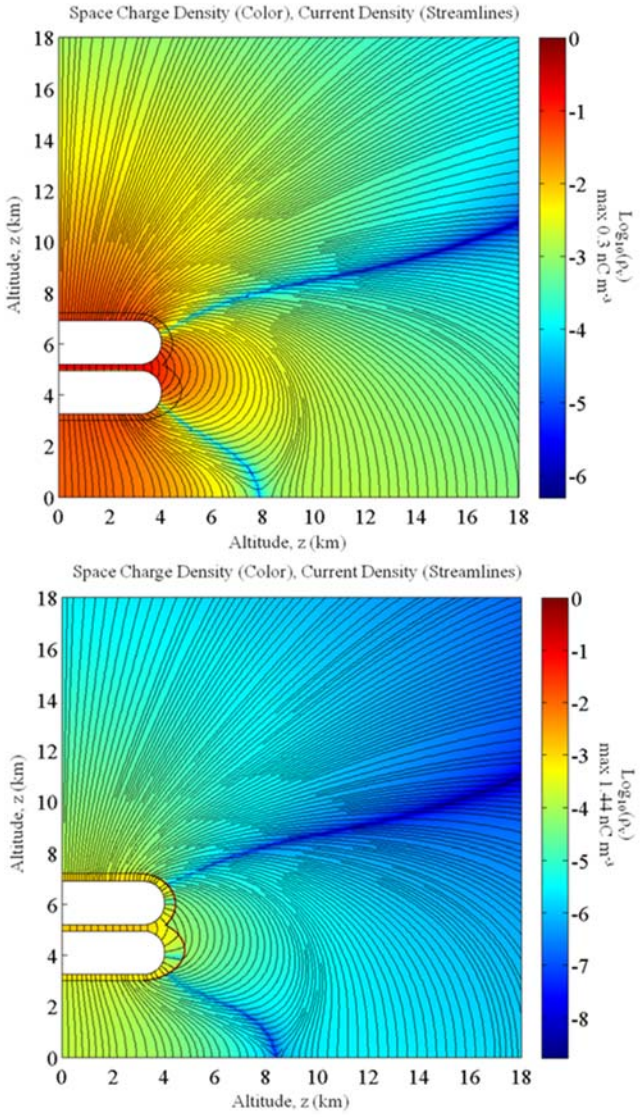

Fig. 10. Space charge density and electric field structure for the ST cloud.

minutes. The electric fields at points 1 through 4 take more time to reach a steady state, and the electric fields at points 5 and 6 reach a steady state more quickly. For the lower conductivity case, the charge centers do not reach a steady-state value before the charging current is turned off at 165 minutes. However, it is evident in Fig. 12b. that the electric field at all six points reaches steady state shortly after at time of 90 minutes or earlier. This analysis exposes a potential weakness of observing the field outside a cloud: electrification of the cloud will appear to have reached a maximum before internal charging is complete, due to the faster relaxation time on the clear-air side of the cloud boundary.

IV. Quantification of Observability Outside the Cloud

The modeling results presented in Section 3 predict that screening layers reduce the electric field magnitude outside a

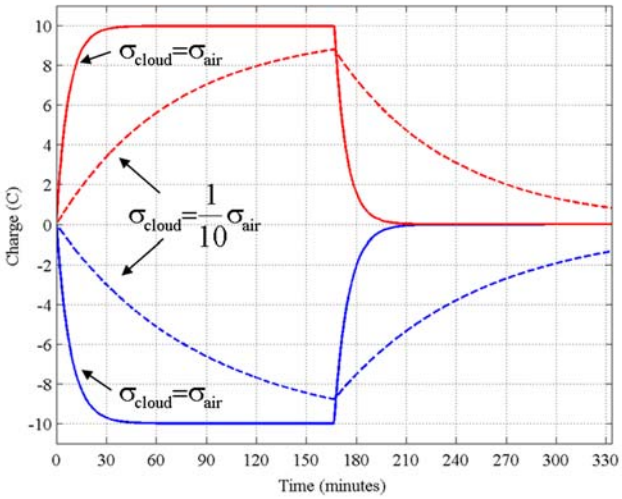

Fig. 11. Time evolution of charge center charge magnitude.

cloud roughly in proportion to the difference in cloud and clear air conductivity, but they have a less significant impact on the structure of the electric field, especially at distances greater than 1 km or so from the cloud boundary. For varying cases of side boundary geometry, charge width, and charge center separation, the electric field probed along our example flight paths generally exhibits the same behavior with similar extrema locations and values. These model results suggest that there could be a useful relationship between the features of the cloud and charge centers and the electric field along the flight paths.

In order to explore potential relationships between cloud features and the electric field outside the cloud, we sampled the spatial location and field values for the 19 extrema points identified in the grey regions of Fig. 5, 7, and 9. The locations and magnitudes of all the maximums and minimums are plotted in Fig. 15 through 19.

Fig. 15 shows plots of the locations and field magnitudes versus the different side boundaries for the extrema at points 1, 2, and 3 (see Fig. 5b and Fig. 5c). Side boundary "0" corresponds to the case of equal cloud conductivity (and thus no cloud boundary at all, see Fig. 3a) and has been reduced by a factor of 10 from its actual value; side boundaries 1 through 5 correspond to the same boundary numbers shown in Fig. 3. Interestingly, even though the side of the cloud boundary is varying by up to 2 km in horizontal extent, the location of the extrema values change no more than 500 m (point 2 for boundary 3), and they change on average by 150 m. The values of Er at point 1 change by several hundred V m^{-1}. The

field values at points 2 and 3 change by, at most, 1 V/m and 3 V/m, or by 8% and 12%, respectively. Therefore, one can conclude from the model results that there are regions outside the cloud where the location and value of maxima are relatively insensitive to the shape of the cloud boundary.

Fig. 16 shows the extrema locations and electric field values for points 4, 5, and 6 (see Fig. 7b and Fig. 7c) along the

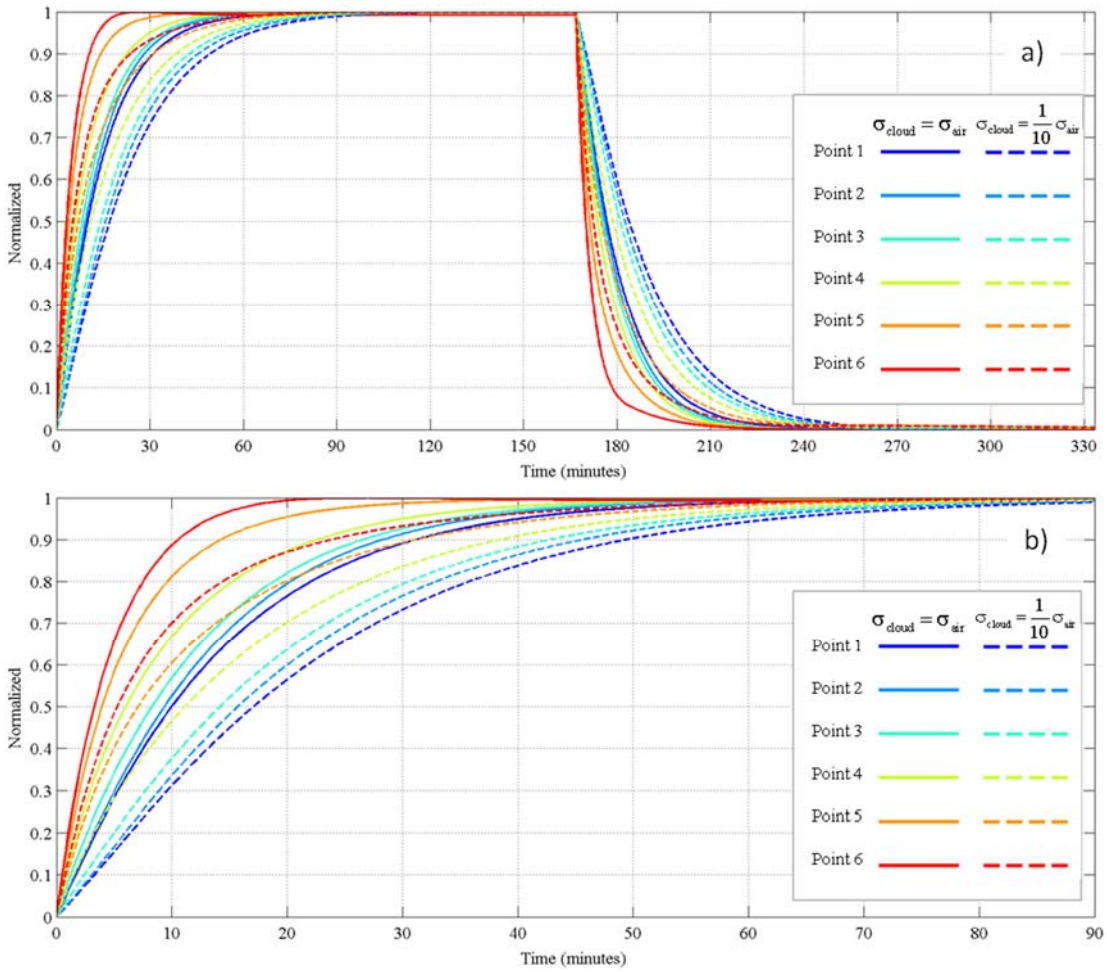

Fig. 12. Time evolution of the electric field at six points shown in Fig. 13

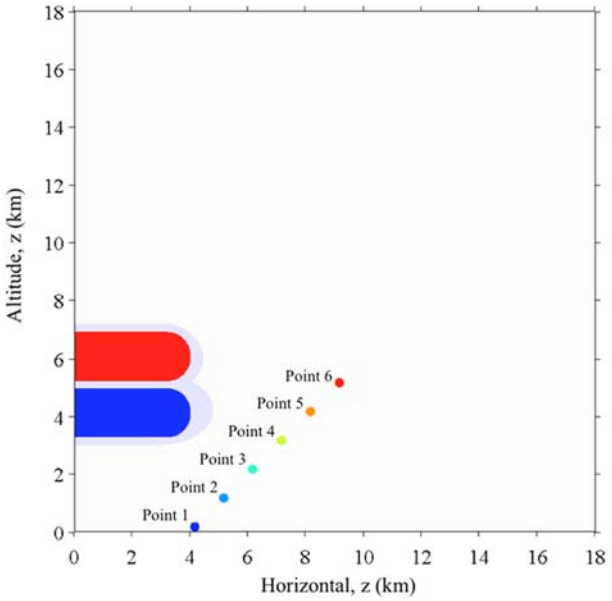

Fig. 13. Field probe locations.

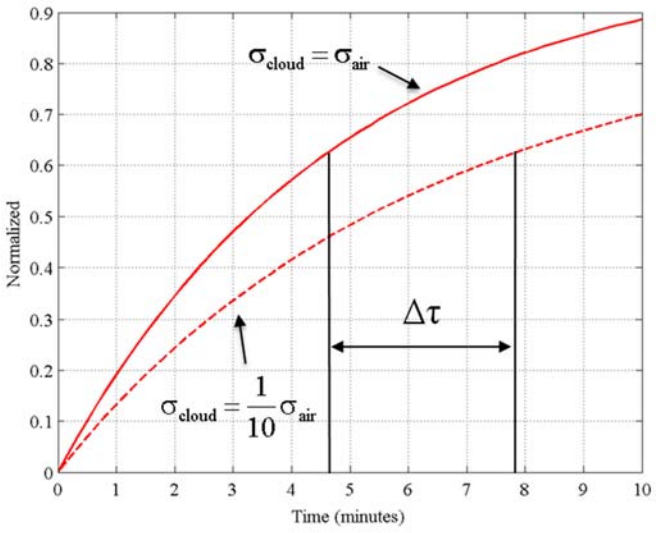

Fig. 14. Expanded view of electric field evolution at point 6.

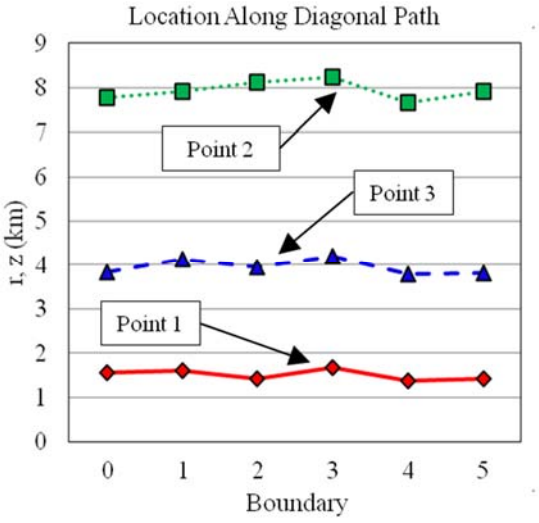

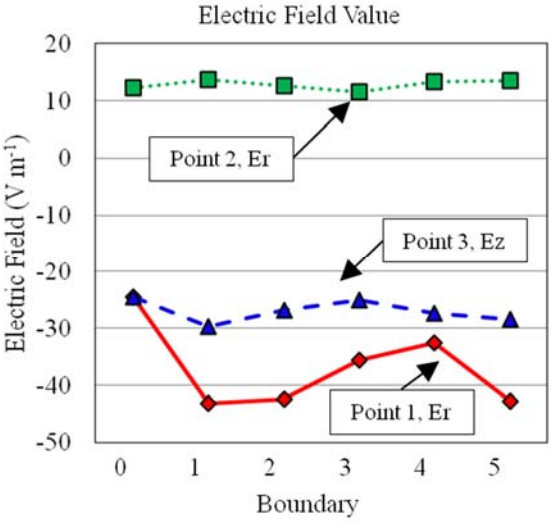

Fig. 15. Locations and values of field extrema for varying side boundaries.

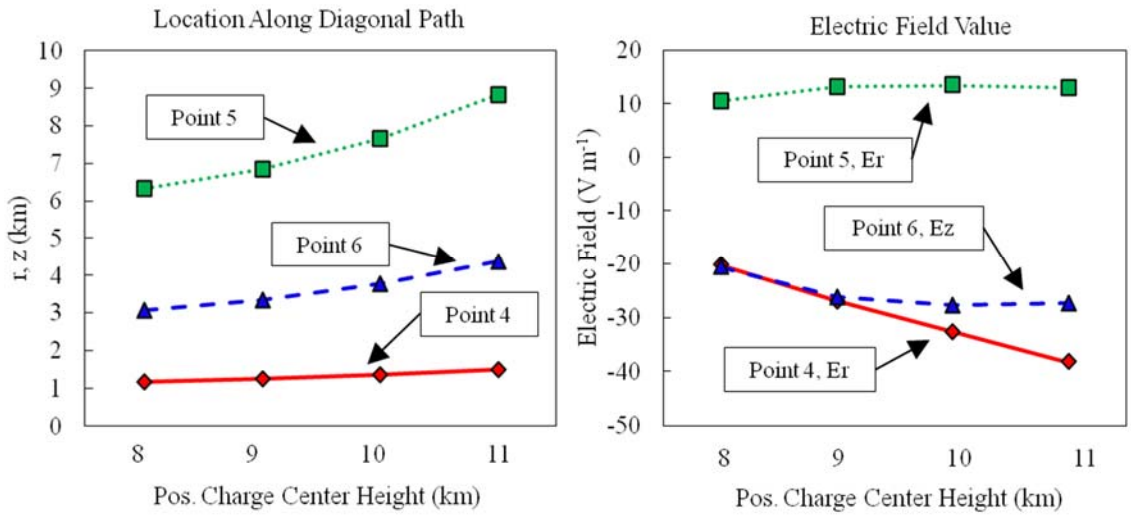

Fig. 16. Locations and values of field extream along the diagonal flight path for varying positive charge center heights.

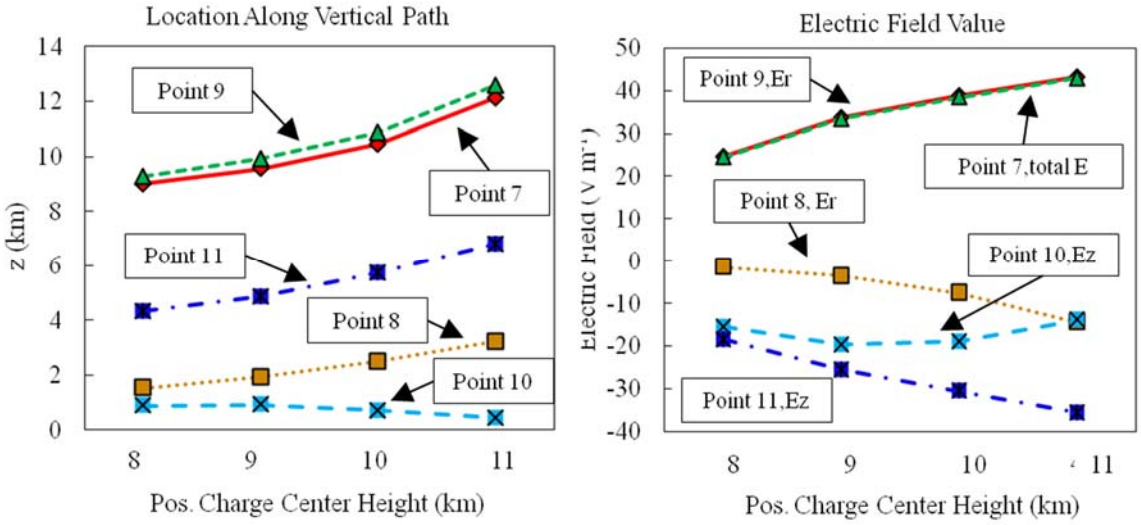

Fig. 17. Location and values of field extrema along the vertical flight path for varying positive charge center heights.

diagonal flight path as the height of the upper positive charge center increases. For all three points, the locations of the extrema increase as the height of the upper charge center increases. Similar results are found for the extrema at points 7, 8, 9, 10, and 11 (see Fig. 7d, Fig. 7e, and Fig. 7f) along the vertical flight path, which are shown in Fig. 17. With the exception of Point 10, the locations of the extrema along the vertical flight path increase in height as the positive charge center height increases. The electric field values at the extrema points change with increasing positive charge center height. These relationships between charge separation and field extrema exist despite the presence and effect of a screening layer.

The values of the extrema along the diagonal and vertical flight paths are plotted against the charge center horizontal extent in Fig. 18 and Fig. 19, respectively. The extrema locations are plotted in the left columns, and the extrema values are plotted in the right columns. At all points, the changes in locations of extrema with increasing charge center width are similar for the equal and lower cases of cloud conductivity. Note that the absolute field values for the equal conductivity case have been reduced by a factor of ten. The changes in extrema field values are also similar for the equal and lower cases of cloud conductivity with the exception of point 12. The percentage change in extrema location as the horizontal charge extent changes is relatively low for points 13, 15, 17, and 19: < 3%, 3.3%, 3.1%, and 8.4%, respectively, for both cases of cloud conductivity. Points 13 and 14 exhibit field changes no greater than 6% and 2.5%, respectively, for both cases of cloud conductivity. These results indicate that the horizontal charge extent has a less significant impact on the electric field structure outside the cloud boundary than does the charge separation.

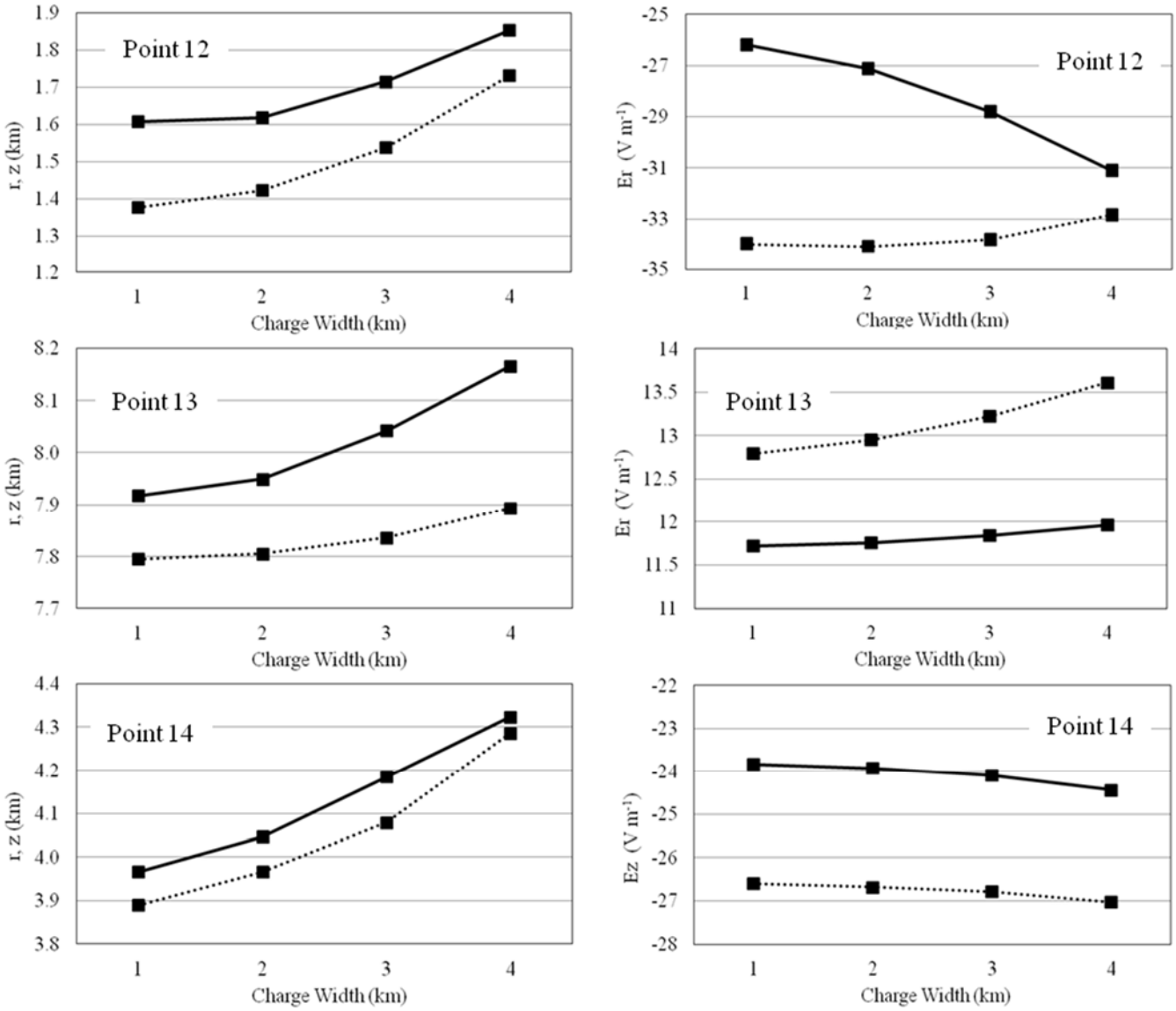

Fig. 18. Locations and values of field extrema along the diagonal path for varying charge widths.

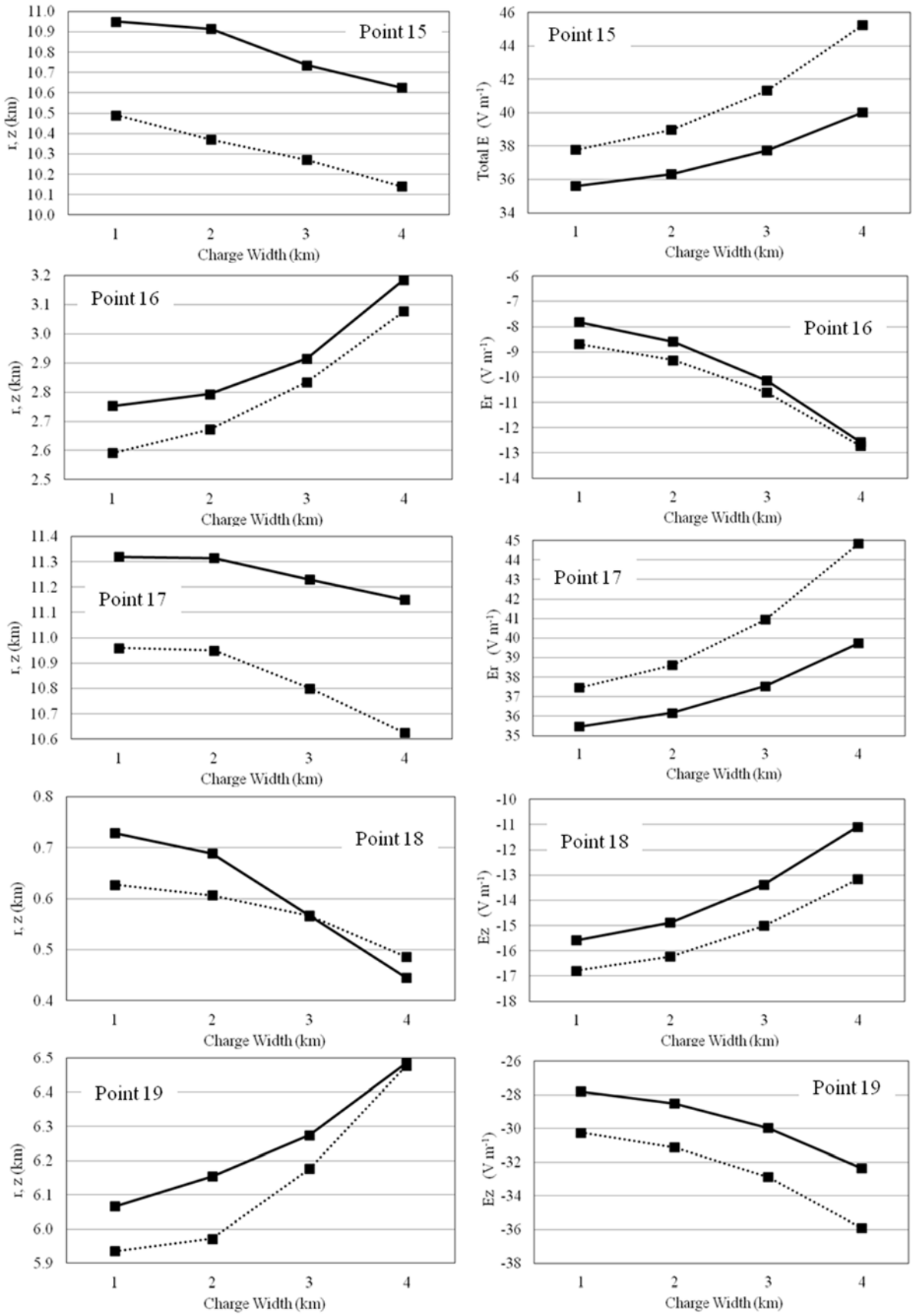

Fig. 19. Locations and values of field extrema along the vertical path for varying charge widths.

V. Discussion

The model results presented in Section 3 and the analysis of field extrema presented in Section 4 suggest that the locations of the charge centers could be inferred with a reasonable degree of certainty from a combination of modeling and measurements of quasi-static electric fields outside of clouds. The modeling results indicate that the screening layer decreases the magnitude of the electric field outside the cloud, but it has a lesser impact on the structure of the electric field. They also indicate that the external fields can be quite small, leading to a requirement for now-noise and sensitive measurements. If these model results reflect reality, then initial cloud charging could be detected by spatially resolved measurements of the electric field outside the cloud. The modeling inferences presented above lead us to conclude that further research into this study is warranted to model more complex charge structures and to measure electric fields outside of electrified clouds.

This paper summarized our initial effort to demonstrate the utility of electric fields measurements made outside of clouds at altitude. To simplify the analysis and interpretation of the results, some processes and features were omitted from or greatly simplified in the modeling. The following is a discussion of the processes and features that will likely have the greatest impact on the modeling results. Perhaps the greatest uncertainty left by this modeling study is the results for clouds having multiple charge centers. We have yet to model three or more charge centers having varying quantities of charge, which will result in a more complex electric field structure, both inside and outside the cloud, and therefore a more complex screening layer. The background current density produced by ionospheric potential, and the current density from corona generated at ground are not included, but they will contribute charge to the screening layer in a manner that may produce more distortion of the electric field structure. We are cautiously optimistic that incorporating more complex charge structures and externally generated current densities into the model will not significantly alter the results of this study; although the complexity of the field structure may increase, it will remain present and exhibit consistent field extrema above the boundary layer. However, it is possible that the distortion due to the screening layer will extend to greater distances from the cloud boundary than for a simple two-charge-center cloud, and that the number of field extrema will increases as well. We modeled CB cloud shapes with side boundaries varying by up to 2 km in a somewhat random manner. Larger variations occur in clouds that will have a greater impact on the electric field structure than smaller variations, but any such variation in a cloud under measurement could be included easily in a model. As the variations on the side boundary become smaller, the cloud shape approaches that of a cylinder, and the screening layer becomes more uniform. We expect the screening layer on variations smaller than those modeled here to have a smaller impact on the electric fields outside of clouds. Cloud dynamics, such as convection through the cloud base and entrainment/detrainment, will impact the screening layer charge in ways that are not incorporated in the model. Updrafts through the cloud base may remove charge or distribute charge over a greater volume in the lower region of the cloud. We have assumed that atmospheric conductivity is independent of polarity. This is not precisely correct, given the roughly 30% higher mobility of negative ions aloft [Nicoll, 2012].

There is significant uncertainty regarding the conductivity inside clouds. We have found reports that it ranges from zero to a factor of ten lower than that of clear air [e.g., MacGorman and Rust 1998]. In our model, the conductivity was ohmic with a simple dependence on altitude, but in reality, the conductivity is likely more non-ohmic and highly heterogeneous. The time evolution of the charge magnitude in the charge centers and the electric field in the model both depended on the conductivity. However, since cloud charging occurs primarily by collisions between cloud precipitates yielding charge separation, rather than a steady current as in the model, it is unclear to what extent conductivity affects charging rates. It is reasonable to expect that electric fields will develop in accordance with the altitude dependent conductivity, but conductivity is dependent on many factors and changes in time. Our results do suggest that given the faster relaxation time outside the cloud boundary, slow electrification due to charge separation within the cloud may not be perceived outside the cloud.

Measurements of the vector electric field aloft are needed in order to confirm any of the model predictions presented here. Deploying small UAV's carrying appropriate electric field sensors is now a practical consideration (see Zhang et al., this conference). Measurements can be used to corroborate modeling results, and also to direct improvements in the accuracy of the modeling. If such an endeavor were successful, then measurements of the electric field outside of clouds at altitude could be used to reliably infer information about the modestly sized internal charge structure, including whether sufficient charge separation, and therefore electric fields, exist in a cloud that could damage aircraft or space vehicles flying through or near it.

Acknowledgment

We thank E. P. Krider, J.C. Willett, and P.R. Krehbiel for helpful discussions during this work.

References

Breed, D. W., and J. E. Dye (1989), The electrification of new-mexico thunderstorms .2. Electric-field growth during initial electrification, J. Geophys. Res., 94(D12), 14841-14854, doi: 10.1029/JD094iD12p14841.

Driscoll, K. T., R. J. Blakeslee, and M. E. Baginski (1992), A modeling study of the time-averaged electric currents in the vicinity of isolated thunderstorms, J. Geophys. Res., 97(D11), 11535-11551.

Dye, J. E., et al. (2007), Electric fields, cloud microphysics, and reflectivity in anvils of Florida thunderstorms, J. Geophys. Res., 112(D11), doi: 10.1029/2006jd007550.

Gunn, R. (1948), Electric field intensity inside of natural clouds, Journal of Applied Physics, 19(5), 481-484, doi: 10.1063/1.1698159.

Gunn, R. (1957), The electrification of precipitation and thunderstorms, Proc. Inst. Radio Eng., 45(10), 1331-1358, doi: 10.1109/jrproc.1957.278220.

Hays, P. B., and R. G. Roble (1979), A quasi-static model of global atmospheric electricity .1. Lower atmosphere, J. Geophys. Res.-Space Physics, 84(NA7), 3291-3305, doi: 10.1029/JA084iA07p03291.

Holzer, R. E., and D. S. Saxon (1952), Distribution of electrical conduction currents in the vicinity of thunderstorms, J. Geophys. Res., 57(2), 207-216, doi: 10.1029/JZ057i002p00207.

Krehbiel, P. R. (1969), Ionic conduction current in thunderstorms, Trans Amer. Geophy. Union, 50(11).

MacGorman, D.R. and W.D. Rust (1998), The Electrical Nature of Storms, Oxford Univ. Press, New York.

Mach, D. M., R. J. Blakeslee, M. G. Bateman, and J. C. Bailey (2009), Electric fields, conductivity, and estimated currents from aircraft overflights of electrified clouds, J. Geophys. Res., 114, doi: 10.1029/2008jd011495.

Marshall, T. C., and W. D. Rust (1991), Electric-field soundings through thunderstorms, J. Geophys. Res., 96(D12), 22297-22306, doi: 10.1029/91jd02486.

Marshall, T. C., and W. D. Rust (1993), 2 types of vertical electrical structures in stratiform precipitation regions of mesoscale convective systems, Bul. Amer. Met. Soc., 74(11), 2159-2170, doi: 10.1175/1520-0477.

Marshall, T. C., W. Rison, W. D. Rust, M. Stolzenburg, J. C. Willett, and W. P. Winn (1995), Rocket and balloon observations of electric-field in 2 thunderstorms, J. Geophys. Res., 100(D10), 20815-20828, doi: 10.1029/95jd01877.

Mo, Q., A. G. Detwiler, J. Hallett, and R. Black (2003), Horizontal structure of the electric field in the stratiform region of an Oklahoma mesoscale convective system, J. Geophys. Res., 108(D7), doi: 10.1029/2001jd001140.

Nicoll, K. A. (2012), Measurements of Atmospheric Electricity Aloft, Surveys in Geophysics, 33(5), 991-1057, doi: 10.1007/s10712-012-9188-9.

Rakov, V.A. and M.A. Uman (2003), Lightning: Physics and Effects, Cambridge Univ. Press, New York.

Rust, W. D., and C. B. Moore (1974), Electrical conditions near bases of thunderclouds over New-Mexico, Quarterly Journal of the Royal Meteorological Society, 100(425), 450-468, doi: 10.1002/qj.49710042516.

Stolzenburg, M., and T. C. Marshall (2008), Charge structure and dynamics in thunderstorms, Space Science Reviews, 137(1-4), 355-372, doi: 10.1007/s11214.

Tzur, I., and R. G. Roble (1985), The interaction of a dipolar thunderstorm with its global electrical environment, J. Geophys. Res., 90(ND4), 5989-5999, doi: 10.1029/JD090i.

Wilson, C. T. R. (1956), A theory of thundercloud electricity, Proc. Roy. Soc. of London, Series A-Mathematical and Physical Sciences, 236(1206), 297-317, doi: 10.1098/rspa.1956.0137.